Available online at www.eccomasproceedia.org
Eccomas Proceedia SMART (2025) 206-217

ECCOMAS
Proceedia

XI ECCOMAS Thematic Conference on Smart Structures and Materials - SMART 2025
M. Krommer, M. Nader and M. Schagerl (Eds)

Received: 28 April 2025 / Revised: 31 August 2025 / Accepted: 3 October 2025
© The Author(s) 2025

A Semi-Active Metastructure System for Vibroacoustic Isolation

Giorgos M. Sarmas, Ilias A. Tsakonas, Dimitris K. Dimitriou, Nikolaos A. Chrysochoidis, Dimitris A. Saravanos, Christoforos S. Rekatsinas

Abstract.
Metastructures have the potential to suppress vibrations by utilizing local resonators tuned to frequencies within a bandwidth near the modal frequencies of the baseline structure. The present vibration suppression mechanism relies on the interaction between the host structure and the local resonators, which act as multiple-tuned mass dampers (TMDs). Unlike a single TMD, multiple TMDs significantly increase the effective frequency range of vibration attenuation, forming a bandgap. Our previous studies [1], [2] demonstrated the effectiveness of a piezoelectric semi-active TMD equipped with an R-L circuit in achieving high and adaptable vibration reduction performance through the judicious selection of the resistive and inductive loads. Building on this foundation, the current work presents a numerical investigation of one-dimensional piezoelectric metastructures. The conceptual framework leverages recent advancements in the 4D printing concept, allowing the development of metastructures equipped with multiple piezoelectric resonators. The numerical models employed in this study encompass simple lumped-mass systems to analyze axial vibrations and beam models to investigate bending vibrations, both incorporating piezoelectric resonators. Each resonator is mechanically tuned to operate at the same modal frequency, and an R-L circuit is connected to its terminals, providing electromechanical coupling capabilities. This integration facilitates the dynamic adjustment of bandgap properties efficiently and effectively. This study aims to investigate the vibration attenuation mechanisms and assess their influence on the structure's steady-state dynamic response by introducing multiple poles and zeros into the electromechanical system. The potential of the current approach, including the ideal number of resonators, the effectiveness of the piezoelectric characteristics, and the influence of circuit parameters, is thoroughly studied.

Key words: piezoelectric resonators, metastructure, tuned mass dampers, bandgap, electromechanical response.

Giorgos Sarmas & Ilias Tsakonas & Dimitris Dimitriou & Nikolaos Chrysochoidis & Dimitris Saravanos
Department of Mechanical and Aeronautical Engineering, University of Patras, Patras University Campus, 26504, Patras, Greece, e-mail: nchr@mech.upatras.gr

Christoforos Rekatsinas
National Center of Scientific Research, Demokritos

ISSN:3078-543X. Published by Eccomas Proceedia.
Peer-review under responsibility of the organizing committee of SMART 2025.
doi: 10.7712/150125.13628.201014

1 INTRODUCTION

In modern engineering applications, the need for effective vibration mitigation and vibration-based energy harvesting has become more critical than ever. Unwanted vibrations and noise not only compromise performance but also increase wear, reduce lifespan and raise safety concerns. As a result, various vibration control strategies have been investigated. A well-established approach is the integration of a baseline structure with passive tuned mass dampers (TMDs) or dynamic vibration absorbers (DVAs) [3].While effective, TMDs typically perform well only at a single resonant frequency, making them unsuitable for broadband vibration control. To address this limitation, they have been coupled with piezoelectric [1], [2] and electromagnetic transducers [4], granting them semi-active characteristics. Shunting these transducers with electrical circuits, the vibration attenuation and energy dissipation can be enhanced by leveraging the circuit's dissipative and dynamic properties. Another widely studied approach involves the bonding of piezoelectric patches on the main structure, giving raise into electromechanical coupling and vibration tailoring [5], [6], [7].

Another promising methodology, which is similar, encompasses the periodical placement of locally resonant elements on the vibrating structure, forming what is known as a metastructure. Through careful parametric tuning of these resonant elements, metastructures can introduce frequency bands where vibration transmission is significantly suppressed, the so-called bandgaps or stopbands. Extensive research has been conducted on achieving both single [8], [9] and multiple bandgaps [10] for beam structures. A basic factor in the procedure of incorporating absorbers is their added mass. In this context, conserved-mass approaches and optimized procedures have been explored for axial [11] and bending vibrations [12] to develop lightweight structures with the proper dynamic responses. Another crucial challenge is the synergy between vibration control and energy harvesting. Over the last decade, research on vibration-based energy harvesting has grown significantly, exploring various energy conversion mechanisms, such as electromagnetic and piezoelectric, tailored to specific applications [13], [14].

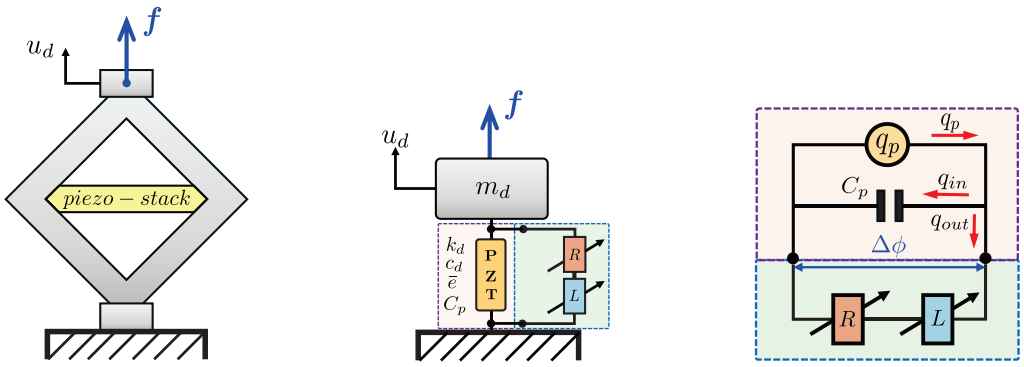
Building on our group's previous research [1], [2], [15], current work explores the attenuation capabilities of multiple semi-active TMDs on uniform bars and beams for axial and bending vibrations, respectively. The physical model of each TMD consists of a diamond-shaped frame equipped with a piezoelectric stack transducer, modelled as a single-degree-of-freedom system. To achieve the semi-active characteristics, a resistor-inductor (RL) circuit is connected to the terminals of the stack. In this way, the whole system acquires electromechanical behavior, leveraging the dissipative and dynamic characteristics of the circuit. The vibration attenuation performance, as well as the efficiency to create tunable vibration bandgaps, will be studied.

2 DYNAMICS OF PIEZOELECTRIC SATMD

The equation of motion of a passive single-degree-of-freedom TMD is:

$$m_d\ddot{u}_d + c_d\dot{u}_d + k_d u_d = f \qquad (1)$$

where $u_d, \dot{u}_d, \ddot{u}_d,$ represent the displacement, velocity, and acceleration responses under the excitation force f. However, for the SATMD, considering that a part of the kinetic energy is converted into electrical at the PZT terminals, the connected spring-damper elements of TMD are replaced with a piezoelectric transducer (PZT), **Figure 1**.



(a) (b) (c)

Figure 1: Modeling of SATMD, (a): Diamond-shaped SATMD, (b): Lumped model, (c): Circuit.

Hence, the equation of motion of the SATMD has the following form:

$$m_d\ddot{u}_d + c_d\dot{u}_d + k_d u_d + \bar{e}\Delta\phi = f \tag{2}$$

With:

$$\begin{cases} f_m = k_d u_d \\ f_e = \bar{e}\Delta\phi \end{cases} \tag{3}$$

Expressing the mechanical f_m and the electrical f_e force generated in the piezoelectric stack [15]. k_d represents the mechanical stiffness of the piezoelectric device, $\bar{e}$ [N/V] stands for the equivalent piezoelectric stress coefficient of the piezoelectric stack, indicating the level of the piezoelectric coupling, and $\Delta\phi$ is the generated voltage due to the direct piezoelectric effect. Examining the electric quantities as presented in **Figure 1**c, a source of electric charge, q_p, is generated from the relative movement of the piezoelectric stack and divided into the one that charges the inherent piezoelectric capacitor, q_{in}, and the one that flows as current in the connected circuit, q_{out}. The equilibrium of electric charges in the circuit is:

$$q_p = q_{in} + q_{out} \tag{4}$$

where:

$$\begin{cases} q_p = \bar{e}u_d \\ q_{in} = C_p\Delta\phi \end{cases} \tag{5}$$

and C_p is the inherent capacitance of the piezoelectric stack. Now we can distinguish between two cases:

Case1: Open Circuit Conditions

If the PZT is in an open-circuit condition ($q_{out} = 0$), this leads only to the charge of the capacitor:

$$q_{in} = q_p \tag{6}$$

and the corresponding equation of motion takes the form:

$$m_d\ddot{u}_d + c_d\dot{u}_d + \left(k_d + \bar{e}^{\,2}/C_p\right)u_d = f \tag{7}$$

The above equation implies that the internal energy of the system is stored in the form of either strain energy in the springs or as electric energy in the piezoelectric element, resulting in a stiffness variation of the system by the piezoelectric coupling term ($\bar{e}^{\,2}/C_p$).

Case2: Shunt Circuit

Shunting the PZT with a resistor and an inductor in series, and applying Kirchhoff's Voltage Law at the respective loops of the circuit, **Figure 1**c:

$$\Delta\phi = L\ddot{q}_{out} + R\dot{q}_{out} = \frac{q_{in}}{C_p} \tag{8}$$

Combining equations (2), (4), and (8), the equations of motion of the shunted SATMD can be written as:

$$\begin{bmatrix} m_d & 0 \\ 0 & L \end{bmatrix}\begin{Bmatrix} \ddot{u}_d \\ \ddot{q}_{out} \end{Bmatrix} + \begin{bmatrix} c_d & 0 \\ 0 & R \end{bmatrix}\begin{Bmatrix} \dot{u}_d \\ \dot{q}_{out} \end{Bmatrix} + \begin{bmatrix} k_p & -\bar{e}/C_p \\ -\bar{e}/C_p & 1/C_p \end{bmatrix}\begin{Bmatrix} u_d \\ q_{out} \end{Bmatrix} = \begin{Bmatrix} f \\ 0 \end{Bmatrix} \tag{9}$$

where $k_p = k_d + \bar{e}^{\,2}/C_p$.

In the above form, one can see that inductance and resistance play the role of phenomenal mass and damping, respectively.

3 DEVELOPMENT OF GLOBAL MATRICES

In the finite element model of the metastructure, the total degrees of freedom (DOFs) consist of (1) the mechanical DOFs of the host structure, (2) the mechanical DOFs of the SATMDs, and (3) the electric DOFs (output electric charges) which arise from the shunted piezoelectric element of each SATMD. Hence, the vector of total DOFs is:

$$\boldsymbol{u_{tot}} = \{\boldsymbol{u}_h, \boldsymbol{u}_d, \boldsymbol{q}\}^{\mathrm{T}}_{(N+2n)\times 1} \tag{10}$$

where N: number of DOFs of the host structure, n: number of SATMDs, $\boldsymbol{u}_h$: mechanical DOFs of the host structure, and $\boldsymbol{u}_d$ & $\boldsymbol{q}$ are the mechanical and electric DOFs of the SATMDs, respectively. For a better understanding of the following procedure, the construction of rod matrices is only presented assuming a single SATMD connected to the 2nd DOF. The addition of multiple SATMDs is similar and easily reproducible. When a SATMD is incorporated into

a host DOF characterized by effective mass m_1, damping c_1 and stiffness k_1, it alters the host DOF dynamics, resulting in a coupled system of equations:

$$\begin{bmatrix} m_1 & 0 & 0 \\ 0 & m_d & 0 \\ 0 & 0 & L \end{bmatrix} \begin{Bmatrix} \ddot{u}_h \\ \ddot{u}_d \\ \ddot{q} \end{Bmatrix} + \begin{bmatrix} c_1 + c_d & -c_d & 0 \\ -c_d & c_d & 0 \\ 0 & 0 & R \end{bmatrix} \begin{Bmatrix} \dot{u}_h \\ \dot{u}_d \\ \dot{q} \end{Bmatrix} + \begin{bmatrix} k_1 + k_p & -k_p & \bar{e}/C_p \\ -k_p & k_p & -\bar{e}/C_p \\ \bar{e}/C_p & -\bar{e}/C_p & 1/C_p \end{bmatrix} \begin{Bmatrix} u_h \\ u_d \\ q \end{Bmatrix} = \begin{Bmatrix} f \\ 0 \\ 0 \end{Bmatrix} \quad (11)$$

where u_h is the host DOF, u_d and q are the mechanical and electric DOFs of the SATMD.

The global unconstrained stiffness matrix of the rod is:

$$[\boldsymbol{K}_0] = \begin{bmatrix} k_0 & -k_0 & 0 & \cdots & 0 \\ -k_0 & 2k_0 & -k_0 & \cdots & 0 \\ 0 & -k_0 & 2k_0 & \cdots & 0 \\ \vdots & \vdots & \vdots & \ddots & -k_0 \\ 0 & 0 & 0 & -k_0 & k_0 \end{bmatrix}_{N \times N} \quad (12)$$

where $k_0 = EA/L_e$, E: Young's modulus, A: cross-section area and L_e the finite element length. The lumped elemental mass matrix is utilized for the lumped rod model, therefore:

$$[\boldsymbol{M}_0] = \text{diag}([m_0, 2m_0, 2m_0, \dots, m_0])_{N \times N} \quad (13)$$

where $m_0 = \rho A L_e/2$, ρ: density.

From Eq. (11) and (12) the whole structure's unconstrained stiffness matrix is:

$$[\boldsymbol{K}] = \begin{bmatrix} k_0 & -k_0 & 0 & \cdots & 0 & 0 & 0 \\ -k_0 & 2k_0 + k_p & -k_0 & \cdots & 0 & -k_p & \bar{e}/C_p \\ 0 & -k_0 & 2k_0 & \cdots & 0 & 0 & 0 \\ \vdots & \vdots & \vdots & \ddots & -k_0 & 0 & 0 \\ 0 & 0 & 0 & -k_0 & k_0 & \vdots & \vdots \\ 0 & -k_p & 0 & 0 & \cdots & k_p & -\bar{e}/C_p \\ 0 & \bar{e}/C_p & 0 & 0 & \cdots & -\bar{e}/C_p & 1/C_p \end{bmatrix}_{(N+2)\times(N+2)} \quad (14)$$

and the mass matrix, Eq. (11) and (13):

$$[\boldsymbol{M}] = diag(\{ m_0, 2m_0, \dots, 2m_0, m_0, m_d, L \}) \quad (15)$$

Rayleigh damping is introduced for the damping matrix of the metastructure, and the steady-state response is calculated via the dynamic stiffness matrix:

$$\boldsymbol{U} = ([\boldsymbol{K}] + j\omega[\boldsymbol{C}] - [\boldsymbol{M}]\omega^2)^{-1}\boldsymbol{F} \quad (16)$$

where $\boldsymbol{U}$: is the complex amplitude vector and $\boldsymbol{F}$: the generalized force vector, $j^2 = -1$.
The outlines represent the contribution of the SATMD dynamics in the already calculated matrices.

4 NUMERICAL CASE STUDIES

Consider a cantilever rod and beam equipped with multiple SATMDs positioned at regular intervals, separated by a distance d, **Figure** 2.

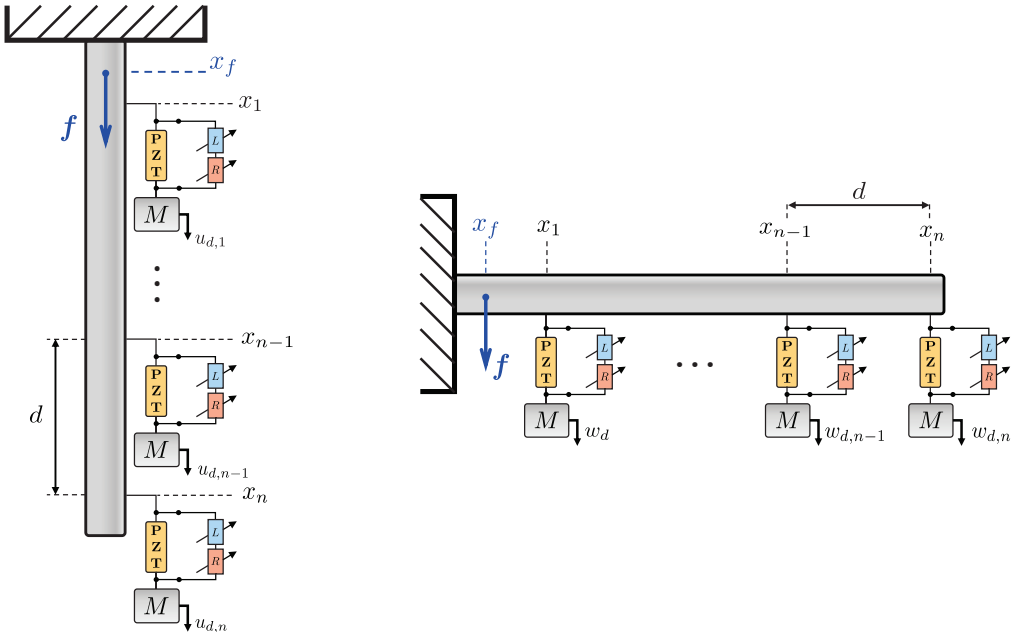


Figure 2: Metastructure models (a): Rod and (b): Beam.

The material properties of the plain structures and the electrical characteristics of commercially available piezoelectrics for the SATMDs are listed in Tables 1 and 2, respectively. The SATMDs are mechanically tuned to the same eigenfrequency for each model, and each unit is shunted to an RL circuit. A harmonic force is applied near the cantilevered end, at $x_f = 0.05$ m. A key parameter in the analysis is the mass ratio:

$$\mu = \frac{\sum_{i=1}^{n} m_{d,i}}{m_{hs}} = \frac{m_{d,tot}}{m_{hs}} \tag{17}$$

where m_{hs} is the host structure mass and $m_{d,tot}$ is the total mass of the absorbers. In this study, the mass ratio is maintained constant, i.e., independent of the number of SATMDs (n). Therefore, $m_{d,i}$ (SATMD mass) and $k_{d,i}$ (SATMD stiffness) must be adjusted appropriately to keep the same SATMD natural frequency as n increases.

Table 1: Geometric and material characteristics of rod and beam

	Length [m]	Height [m]	Width [m]	Young's Modulus [GPa]	Density [kg/m^3]
Rod	1	0.025	0.05	70	2800
Beam	1	0.0167	0.667	70	2800

Table 2: SATMDs characteristics

	$\bar{e}$ [N/V]	C_p [μF]
Rod SATMD	5	2.2
Beam SATMD	0.2	2.2

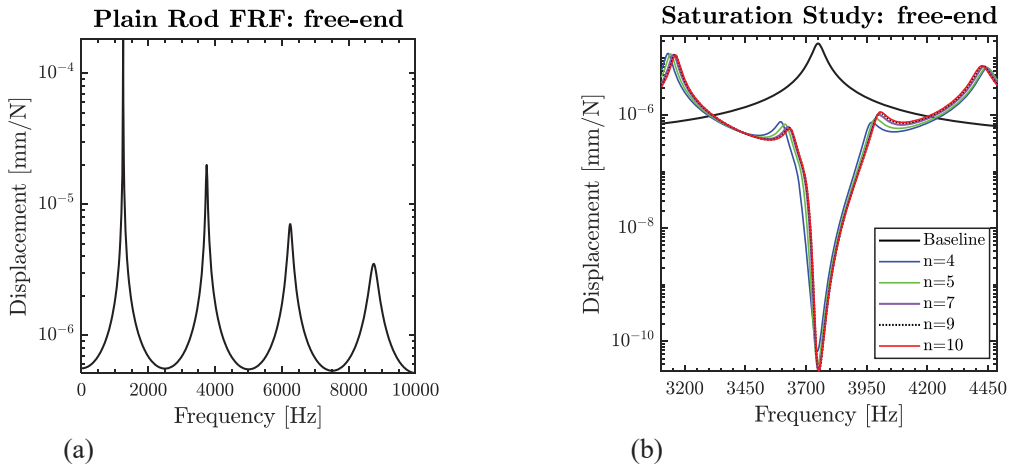


Figure 3: Rod FRFs at its free-end (a): Plain rod, (b): Saturation study at the rod's 2nd mode.

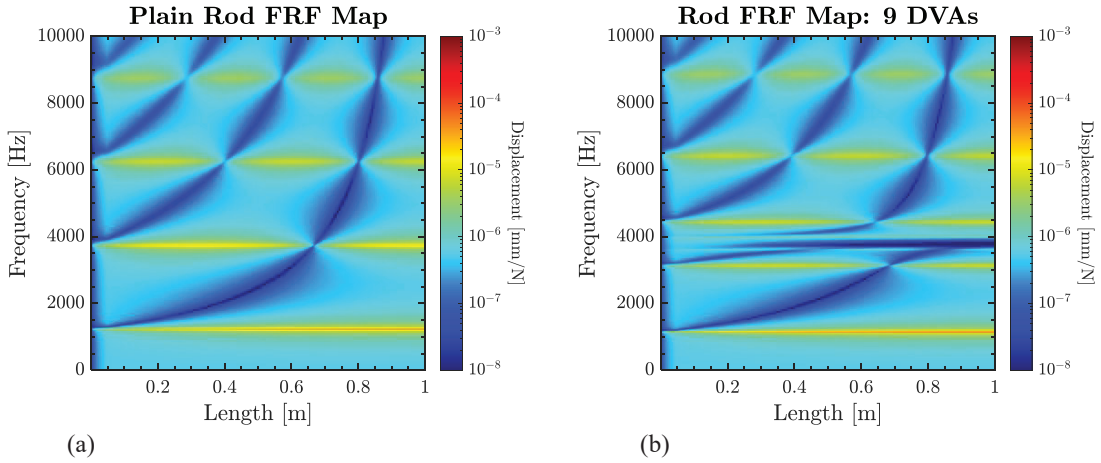


Figure 4: Rod FRF maps, (a): Baseline, (b): Rod with 9 SATMDs.

4.1. Rod with multiple SATMDs

The forced response of the plain rod of **Figure 2**a was simulated at the free end and is presented in **Figure 3**a. This case study aims to suppress the second and third vibration modes. Additionally, introducing the vibration suppression configuration influences the structure's

global dynamic characteristics, which will be investigated to ensure a holistic understanding of the system's performance. Specifically, each of the added SATMDs was tuned at the second mode (3750 Hz) via selecting the appropriate stiffness as the mass ratio μ was set at 0.1. A saturation study is conducted to determine an optimal number of SATMDs [9] and is illustrated in **Figure 3**b.

Based on this study, nine SATMDs were modelled on the rod with $x_1 = 0.285$ m and $d = 0.0894$ m. Aiming to provide a more detailed demonstration of the plain rod's dynamic response **Figure 4**a presents a spatial representation of the FRFs, serving as a baseline reference. On the other hand, **Figure 4**b demonstrates the metastructure's dynamic response. The emergence of an oscillatory bandgap centered around 3750 Hz is obvious, with an estimated bandwidth of 200 Hz and spatial coverage of approximately 0.5 meters. Notably, the bandgap intensity increases with distance from the point of excitation.

Beyond passive tuning, electromechanical coupling is introduced by equipping each SATMD with identical inductors. This generates additional dynamics through electric poles and zeros that arise from the inductors. **Figure 5**a illustrates how the free-end bandgap bandwidth evolves under varying inductance, assuming negligible resistance. Two key effects are observed: (1) the electrically introduced antiresonance creates a new bandgap (right antiresonance zone), passing from higher to lower frequencies while its bandwidth gradually increases, and (2) the mechanical bandgap (left antiresonance zone) is also moving downward in frequency, but its bandwidth progressively decreases. The electric component tends to stabilize in frequency at higher inductance values while the mechanical component gradually diminishes. The reason is that the current flowing through the inductor (for negligible resistance) is:

$$I_{out} = \frac{\Delta\phi}{j\omega L} \to 0 \quad \text{as} \quad L \text{ increases}, \qquad j^2 = -1 \tag{18}$$

This drives the PZT into an open-circuit (OC) condition, decreasing its effective stiffness. These phenomena demonstrate the potential of electromechanical coupling in tuning the bandgap locations and enhancing vibration suppression, providing added flexibility in controlling the system's dynamic response.

The next objective is to suppress vibrations at the free-end corresponding to the third mode, at 6450 Hz, with the set of resonators mechanically tuned at 2nd mode. As shown in **Figure 5**a the right-side antiresonance crosses 6450 Hz when the inductance is approximately 380μH. At this value, two electromechanical bandgaps emerge: one centered at 6450 Hz and another appearing at 3230 Hz. It is evident that the appropriate selection of the connected inductance can tune the desired mechanical bandgap to alternative frequency ranges. The 2nd available tuning parameter is the resistance. In this case, increasing the resistance causes the bandgap to shift toward higher frequencies as higher resistance values gradually drive PZT into OC condition, **Figure 5**b. Interestingly, an optimal resistance, $R = 5\Omega$, yields substantial simultaneous attenuation for both the 2nd and 3rd modes, **Figure 5**c. These results highlight the potential of inductance and resistance regulation as an effective tool for adaptive vibration suppression.

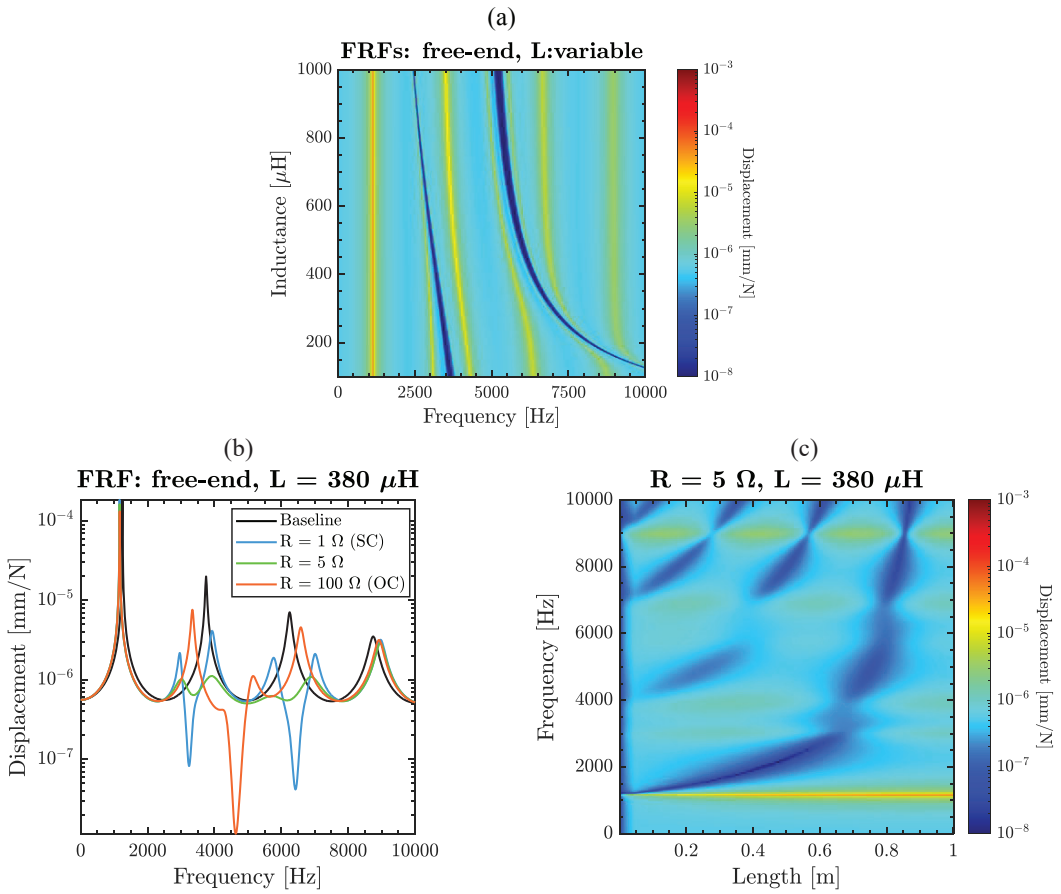


Figure 5: Metastructure Rod FRFs, (a): Frequency-Inductance-Displacement map at rod's free-end, (b): FRFs at rod's free-end with variable resistance, (c): FRF map for whole structure.

4.2. Beam with multiple SATMDs

In the context of the current case study, the oscillatory performance of the beam **Figure 2**b is studied. The dynamic response for the normal displacement of the plain beam at the tip is illustrated in **Figure 6**a, serving as a baseline response. Similar to the rod study case, the objective here is to suppress both the third and fourth natural frequencies at the beam tip. With $\mu = 0.1$, the saturation study determined that eight SATMDs can create a stable mechanical bandgap centered around the 3rd natural frequency at 237 Hz. The 8 SATMDs were positioned with $x_1 = 0.23m$ and $d = 0.11m$. Implementing the SATMDs shifts the fourth natural frequency from 465 to 475 Hz, as observed in **Figure 6**b, while **Figure 6**c demonstrates the variation of electromechanical bandgaps simulated at the beam tip as a function of the connected inductance to the terminals of each SATMD. Based on this analysis, an inductance value of 55 mH is selected to suppress the modal response at 475 Hz effectively.

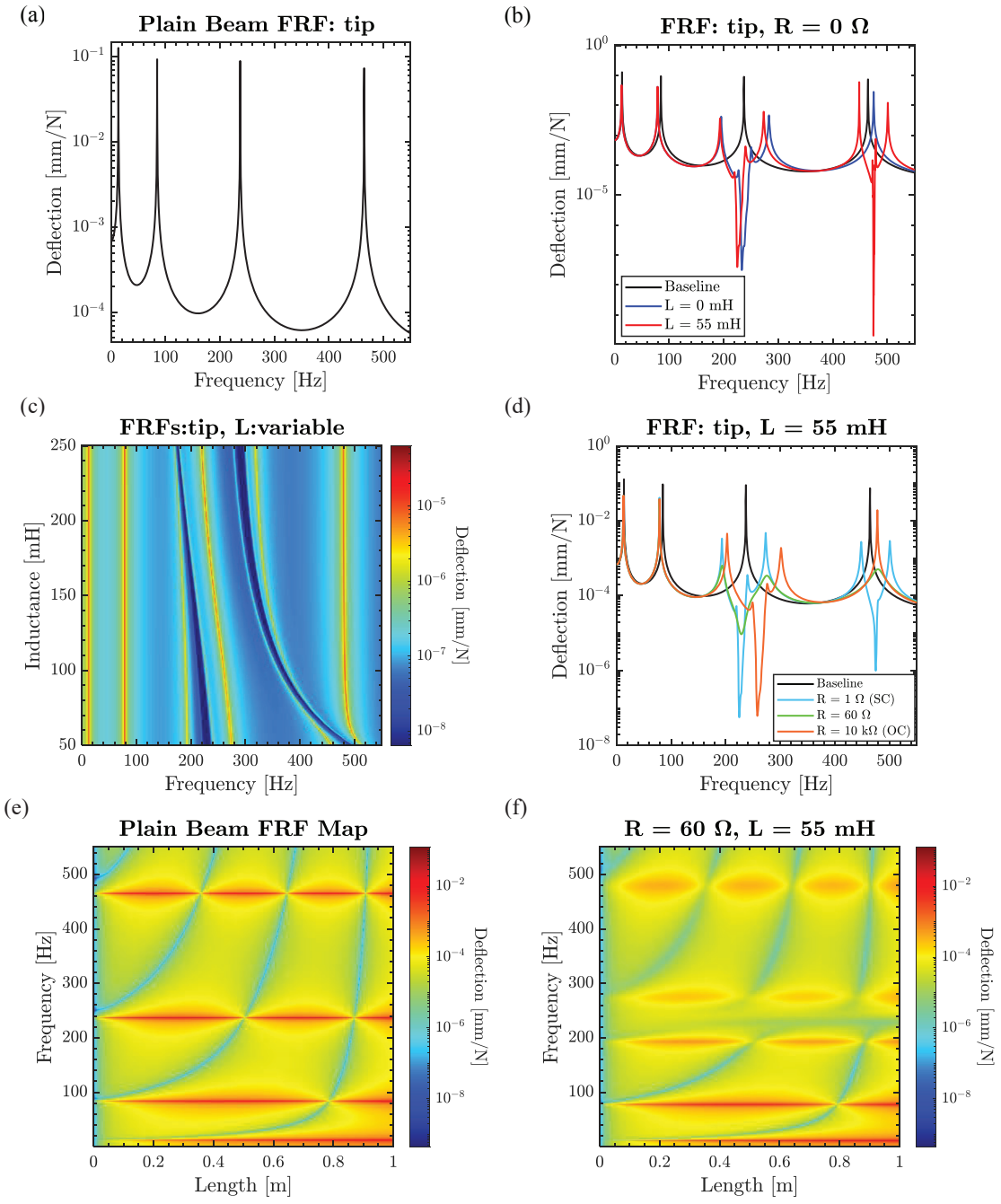


Figure 6: Beam FRFs, (a): Plain beam FRF at the tip, (b): Metabeam FRF at the tip for different inductance values, (c) Metabeam FRF map with variable inductance for the tip, (d) Metabeam FRF at the tip for different resistance values, (e) Plain beam FRF map for whole structure, (f): Metabeam FRF map for whole structure.

With a fixed inductance value, the attention is focused on the connected resistance, selecting three resistance values: $R = 1\Omega$ for SC conditions, $R = 60\,\Omega$ as an optimal value and finally $R = 10k\Omega$ for the OC. For these values, the free end, normal displacement FRFs are presented in **Figure 6**d. Spatial representation of the dynamic response is performed in **Figure 6** e and f correlating the plain beam with the beam equipped with the set of 8 SATMDs, respectively. These figures demonstrate the drastic attenuation achieved across the length of the beam for all the frequency range exceeding the 3rd modal frequency.

5 CONCLUSIONS

This study demonstrated the effectiveness of SATMDs in suppressing targeted vibration modes in beam and rod structures through mechanical and electromechanical tuning. Initially, passive suppression was achieved by aligning the mechanical bandgaps with the targeted natural frequencies. A saturation study confirmed that nine SATMDs were necessary for the rod and eight for the beam, with a 10% mass ratio, ensuring lightweight feasibility. The introduction of electromechanical coupling by integrating an RL circuit into each SATMD, enabled further flexibility in tuning the dynamic response. Inductance variation allowed for the creation and repositioning of additional bandgaps, while resistance regulation provided significant damping effects. The resulting frequency shifts, including the ability to move bandgaps to higher or lower frequencies, highlight the adaptive nature of this approach. In the rod case, the second and third vibration modes were successfully suppressed through appropriate combinations of inductance and resistance, with optimal performance observed at 380 μH and 5 Ω, respectively. Similarly, in the beam case, the third and fourth modes were attenuated, with 55 mH inductance and 60 Ω resistance, providing effective suppression. Overall, the results confirm that electromechanical tuning via multiple SATMDs offers a promising and versatile solution for adaptive vibration control in lightweight structural applications. The method provides precise control over bandgap location and bandwidth, enabling suppression of multiple vibration modes with minimal added mass.

ACKNOWLEDGMENTS

This work is funded by the research project 4D-PIEZOUMME that is implemented in the framework of H.F.R.I call “Basic research Financing (Horizontal support of all Sciences)” under the National Recovery and Resilience Plan “Greece 2.0” funded by the European Union – NextGenerationEU (H.F.R.I. Project Number: 16580).

Further support was provided by the funding program “MEDICUS”, of the University of Patras

REFERENCES

[1] G. M. Chatziathanasiou, N. A. Chrysochoidis, and D. A. Saravanos, “A semi-active shunted piezoelectric tuned mass damper for robust vibration control,” *Journal of Vibration and Control*, vol. 28, no. 21–22, pp. 2969–2983, Nov. 2022, doi: 10.1177/10775463211026487.

[2] G. M. Chatziathanasiou, N. A. Chrysochoidis, C. S. Rekatsinas, and D. A. Saravanos, “A semi-active shunted piezoelectric tuned-mass-damper for multi-modal vibration control of large flexible structures,” *J Sound Vib*, vol. 537, p. 117222, Oct. 2022, doi: 10.1016/j.jsv.2022.117222.

[3] S. Elias and V. Matsagar, “Research developments in vibration control of structures using passive tuned mass dampers,” *Annu Rev Control*, vol. 44, pp. 129–156, 2017, doi: 10.1016/j.arcontrol.2017.09.015.

[4] M. Auleley, O. Thomas, C. Giraud-Audine, and H. Mahé, “Enhancement of a dynamic vibration absorber by means of an electromagnetic shunt,” *J Intell Mater Syst Struct*, vol. 32, no. 3, pp. 331–354, Feb. 2021, doi: 10.1177/1045389X20957097.

[5] O. Thorp, M. Ruzzene, and A. Baz, “Attenuation and localization of wave propagation in rods with periodic shunted piezoelectric patches,” *Smart Mater Struct*, vol. 10, no. 5, pp. 979–989, Oct. 2001, doi: 10.1088/0964-1726/10/5/314.

[6] L. Airoldi and M. Ruzzene, “Wave Propagation Control in Beams Through Periodic Multi-Branch Shunts,” *J Intell Mater Syst Struct*, vol. 22, no. 14, pp. 1567–1579, Sep. 2011, doi: 10.1177/1045389X11408372.

[7] S. Manzoni, M. Berardengo, F. Boccuto, and M. Vanali, “Piezoelectric-shunt-based approach for multi-mode adaptive tuned mass dampers,” *Mech Syst Signal Process*, vol. 200, p. 110537, Oct. 2023, doi: 10.1016/j.ymssp.2023.110537.

[8] C. Sugino, S. Leadenham, M. Ruzzene, and A. Erturk, “On the mechanism of bandgap formation in locally resonant finite elastic metamaterials,” *J Appl Phys*, vol. 120, no. 13, Oct. 2016, doi: 10.1063/1.4963648.

[9] R. Yazbeck, R. Fernandes, J. G. Boyd, D. C. Lagoudas, and S. El-Borgi, “Effect of resonator location and boundary conditions on bandgap formation in a locally resonant beam metastructure,” *Mechanics of Advanced Materials and Structures*, pp. 1–10, Jan. 2025, doi: 10.1080/15376494.2025.2452369.

[10] S. El-Borgi, R. Fernandes, P. Rajendran, R. Yazbeck, J. G. Boyd, and D. C. Lagoudas, “Multiple bandgap formation in a locally resonant linear metamaterial beam: Theory and experiments,” *J Sound Vib*, vol. 488, p. 115647, Dec. 2020, doi: 10.1016/j.jsv.2020.115647.

[11] K. K. Reichl and D. J. Inman, “Lumped mass model of a 1D metastructure for vibration suppression with no additional mass,” *J Sound Vib*, vol. 403, pp. 75–89, Sep. 2017, doi: 10.1016/j.jsv.2017.05.026.

[12] E. E. Basta, M. Ghommem, and S. A. Emam, “Vibration suppression and optimization of conserved-mass metamaterial beam,” *Int J Non Linear Mech*, vol. 120, p. 103360, Apr. 2020, doi: 10.1016/j.ijnonlinmec.2019.103360.

[13] Q. Cai and S. Zhu, “The nexus between vibration-based energy harvesting and structural vibration control: A comprehensive review,” *Renewable and Sustainable Energy Reviews*, vol. 155, p. 111920, Mar. 2022, doi: 10.1016/j.rser.2021.111920.

[14] M. A. Mangi *et al.*, “Applications of piezoelectric-based sensors, actuators, and energy harvesters,” *Sensors and Actuators Reports*, vol. 9, p. 100302, Jun. 2025, doi: 10.1016/j.snr.2025.100302.

[15] G. Chatziathanasiou, “Development and application of a novel semi-active piezoelectric tuned mass damper for robust vibration control of flexible structures with focus on airframe structures,” University of Patras, Department of Mechanical Engineering & Aeronautics, Division of Applied Mechanics, Technology of Materials and Biomechanics, Applied Mechanics Laboratory, 2024. doi: 10.12681/eadd/57187.